INSTITUTE OF PHYSICS PUBLISHING PHYSICAL BIOLOGY

Phys. Biol. **3** (2006) 107–120 doi:10.1088/1478-3975/3/2/003

Embryonic pattern scaling achieved by oppositely directed morphogen gradients

Peter McHale, Wouter-Jan Rappel and Herbert Levine

Department of Physics and Center for Theoretical Biological Physics, University of California, San Diego, La Jolla, CA 92093-0374, USA

Received 19 December 2005
Accepted for publication 18 April 2006
Published 16 May 2006
Online at stacks.iop.org/PhysBio/3/107

Abstract

Morphogens are proteins, often produced in a localized region, whose concentrations spatially demarcate regions of differing gene expression in developing embryos. The boundaries of gene expression are typically sharp and the genes can be viewed as abruptly switching from on to off or vice versa upon crossing the boundary. To ensure the viability of the organism these boundaries must be set at certain fractional positions within the corresponding developing field. Remarkably this can be done with high precision despite the fact that the size of the developing field itself can vary widely from embryo to embryo. How this scaling is accomplished is unknown but it is clear that a single morphogen gradient is insufficient. Here we show how a pair of morphogens A and B, produced at opposite ends of a one-dimensional developing field, can solve the pattern-scaling problem. In the most promising scenario the morphogens interact via an effective annihilation reaction $A + B \rightarrow \emptyset$ and the switch occurs according to the absolute concentration of A or B. We define a scaling criterion and show that morphogens coupled in this way can set embryonic markers across the entire developing field in proportion to the field size. This scaling occurs at developing-field sizes of a few times the morphogen decay length. The scaling criterion is not met if instead the gradients couple combinatorially such that downstream genes are regulated by the ratio A/B of the morphogen concentrations.

1. Introduction

Morphogen gradients play a crucial role in establishing patterns of gene expression during development. These patterns then go on to determine the complex three-dimensional morphology that is needed for organism functionality. Because not all environmental variation can be controlled, gene patterning must be robust to a variety of perturbations, i.e. must compensate for the unpredictable [1].

One aspect of this robustness is size scaling. Typically, gene patterns are established in proportion to the (variable) size of the nascent embryo. A dramatic demonstration of this was made recently in the case of *Drosophila* where the posterior boundary of the *hunchback* gene expression domain was shown to scale (to within 5%) with embryo size [2]. In the standard model of pattern formation in developmental biology, cells acquire their positional information by measuring the concentration of a morphogen gradient and comparing it to some hard-wired set of thresholds [3–5]. As the simplest single-source diffusing morphogen gradient with fixed thresholds clearly does not exhibit this type of proportionality, it is clear that more sophisticated dynamics must be responsible for the observed structures [6]. Unfortunately, little to nothing is known experimentally about how this pattern scaling comes about.

As a first step in deciphering what these more complex processes might entail, we study here the issue of how two morphogen gradients, directed from opposite ends of a developing field, may solve the pattern-scaling problem [3]. Operationally, opposing gradients may arise in developing systems in at least two ways. First mRNA, from which protein is translated, may be anchored at opposite ends of the region in question. As an example, in the *Drosophila* syncytium an anterior-to-posterior gradient is established by the localization of *bicoid* mRNA to the anterior, while *nanos* mRNA localized at the posterior defines a reciprocal gradient [7]. Second, proteins may be secreted by clusters of cells with separate clusters located at opposite ends of the developing field [8]. Both cases may be modelled by the injection of a flux of A and B morphogens at opposite extremities of a

finite domain. We assume that creation of morphogens in the interior of this domain is negligible. We further assume that the morphogen reaches neighbouring cells by an effective diffusion process, thereby creating a gradient [9, 10]. Finally, although time-dependent effects in development patterning might be important in some contexts [11, 12], we assume here that a steady-state analysis is sufficient for scaling of patterns with system size.

We consider two mechanisms in which a pair of morphogen gradients transmits size information to the developmental pattern. The first mechanism, which uses the concentrations of both gradients combinatorially, is an alternative to the simple gradient mechanism [13]. In this mechanism there exist overlapping DNA-binding sites of species A and B in the cis-regulatory modules of the target genes. (We note that in the *Drosophila* syncytium some *krüppel* binding sites overlap extensively with *bicoid* sites [13, 14].) One of the morphogens acts as a transcriptional activator, the second occludes the binding site of the first, and the target gene expression is switched according to the relative concentrations of the two species [15]. In the second mechanism protein B inhibits the activity of transcription factor A by irreversibly binding to it. The interaction is described by the annihilation reaction $A + B \to \emptyset$. The target gene measures the absolute value of the A concentration as in the standard model of developmental patterning; the B gradient serves only to provide size information to the A concentration field.

We should point out two independent studies that appeared after the completion of our work.

In the first instance Howard and ten Wolde [16] examined the *bicoid-hunchback* system in developing *Drosophila* embryos. Their model is in essence the annihilation mechanism mentioned above. They consider an activator gradient originating from one end of the embryo and hypothesize a co-repressor gradient originating from the opposite end. The co-repressor can bind to the activator, thereby inhibiting its transcriptional ability. They show that their model naturally leads to expression boundaries that are precisely at the centre of the embryo. Furthermore, they demonstrate that this pattern scales with the embryo size and is quite robust to variations in the synthesis rates of the activator and co-repressor. Compared to the study presented here, their model is biochemically more detailed and mathematically more complex, although their results are quite general. The relative simplicity of our model is its main strength, as it lends itself to rigorous mathematical analysis.

In the second instance Houchmandzadeh and co-workers [17] investigated the combinatorial mechanism mentioned above, also in the context of the early *Drosophila* embryo. The authors demonstrate that two morphogen gradients can account for most of the experimental data. They consider the effect of changing *bicoid* copy number and point out that the resultant shift in the Hunchback boundary is twice as small in the combinatorial model as it is in the single-gradient model, thereby bringing the theoretical prediction into line with the experimental data. Importantly they also show how a combinatorial model can determine the midpoint of the embryo reliably even in the presence of a temperature step centred on the embryo, as recently demonstrated experimentally [18]. Their argument is based on the fact that a reduction in synthesis rate due to a lowering of temperature is accompanied by an increase in the diffusion length. These effects can cancel at mid-embryo so that the numbers of A and B molecules reaching the centre of the embryo are the same.

The goal of this work is to study the combinatorial and annihilation mechanisms in their most general setting to see the extent to which they do in fact solve the pattern scaling problem. To this end we measure the range of variables over which scaling is approximately valid. We begin in section 2 by pointing out that a single gradient in a finite system cannot set markers in proportion to the size of the developing field. In section 3 we study the case of two gradients whose binding sites overlap and show that approximate scaling then occurs in a fraction of the developing field typically located midway between the sources. We then turn to the annihilation model of two gradients in section 4 and show that its scaling performance is excellent throughout the developing field.

2. Single gradient

Let A be the concentration of the morphogen which in the simplest model obeys

$$0 = D_a \partial_x^2 A - \beta_a A \tag{1}$$

at steady state. Here D_a is the diffusion constant of protein A and β_a is the degradation rate. Molecules of A are injected at the left boundary with rate Γ_a and are confined to the interval $[0, L]$ by a zero-flux boundary condition

$$-D_a \partial_x A(0) = \Gamma_a, \qquad -D_a \partial_x A(L) = 0. \tag{2}$$

The obvious solution is

$$A = \frac{\lambda_a \Gamma_a}{D_a}\left[\sinh\left(\frac{L}{\lambda_a}\right)\right]^{-1} \cosh\left(\frac{L-x}{\lambda_a}\right) \equiv A(L)\cosh\left(\frac{L-x}{\lambda_a}\right). \tag{3}$$

The length scale λ_a is defined by $\lambda_a = \sqrt{D_a/\beta_a}$.

Let us assume that the boundary between different gene expression regions is determined by the position x_t at which A equals some threshold value A_t. Inverting, the expression for the threshold position is

$$x_t(L) = L - \lambda_a \cosh^{-1}(A_t/A(L)). \tag{4}$$

Note that there is a minimum system size for a specific threshold,

$$L_m = \lambda_a \sinh^{-1}\left(\frac{\lambda_a \Gamma_a}{D_a A_t}\right), \tag{5}$$

such that $x_t(L_m) = L_m$. When $L - x_t \gg \lambda_a$ the concentration profile becomes purely exponential and $x_t \to x_\infty$ where

$$x_\infty = \lambda_a \ln\left(\frac{\lambda_a \Gamma_a}{D_a A_t}\right). \tag{6}$$

Consider the functional form of $x_t(L)$. For L smaller than L_m the function is undefined. At $L = L_m$ its value is $x_t = L_m$. As L is increased further x_t decreases and asymptotically

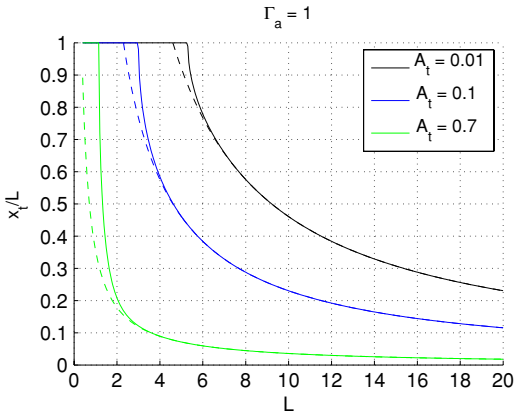

Figure 1. A single gradient is insufficient to scale expression boundaries with developing-field size. Shown is the dependence of normalized x_t on system length L for the case of a single gradient. The solid lines are the analytic expressions (4) for x_t/L for values of the threshold concentration equal to (from top to bottom) $A_t = 0.01$, 0.1, 0.7. Dashed lines are x_∞/L curves as given by (6). All parameters are unity unless otherwise stated.

approaches x_∞, which is always less than or equal to L_m. In other words x_t is always greater than x_∞; this is because the effect of the zero-flux boundary condition is to make x_t larger than it would be in the absence of the boundary. Figure 1 shows the variation of x_t/L with L for three different values of the threshold concentration A_t. Perfect scaling would correspond to $x_t/L \sim$ constant. At the other extreme the complete absence of scaling manifests itself in $x_t/L \sim x_\infty/L$. As is clearly seen the actual x_t/L curves are everywhere close to x_∞/L curves and are nowhere close to constants. We conclude that a single gradient is insufficient to scale markers with developing field size.

3. Combinatorial model

We next ask whether a molecular mechanism that computes the expression level of a target gene based on the concentrations of two different morphogens can lead to gene expression boundaries that scale with system size.

Consider a cis-regulatory module in which the fold change in transcription initiation $F(A, B)$ is determined by the concentrations of transcription factors A and B [15]. The fold change is the ratio of the probability that RNA polymerase is bound to the DNA in the presence of transcription factors to the probability that it is bound in the absence of transcription factors. We neglect the effect of post-transcriptional gene regulation and make the gross assumption that the fold change in transcription initiation is representative of the ultimate fold change in gene expression. A reasonable definition of the boundary between the 'on' and 'off' expression states is $F(A, B) = 0.5 * F_{\max}$ where $F_{\max}$ is the largest fold change possible.

Consider also the case where the spatial profiles of the transcription factors A and B are inhomogeneous. Suppose we write both $A(x)$ and $B(x)$ in terms of the scaled position $\overline{x} = x/L$ and the system size L. For each $\overline{x}$ between 0 and 1 there is a curve $(A(\overline{x}, L), B(\overline{x}, L))$ in the A–B plane parametrized by L.

The general condition then that must be met to obtain size scaling in this two-component combinatorial model is as follows. A pair of morphogen gradients will scale the expression boundary (at a scaled position $\overline{x}$) of a given gene provided the parametric curve $(A(\overline{x}, L), B(\overline{x}, L))$ coincides with the half-maximal contour of the fold-change function $F(A, B)$ corresponding to that gene. To illustrate the point we consider in the following a particular cis-regulatory architecture within a thermodynamic framework [15]. We then couple the resulting fold-change function to space via a pair of exponentially distributed morphogen gradients.

Consider a gene whose cis-regulatory region contains a binding site for a transcription factor A. This binding site overlaps that of another transcription factor B. The factor B does not recruit the RNA polymerase to the promoter (i.e. it is not an activator) and its binding site does not overlap the promoter (i.e. it is not a repressor). Instead B regulates transcription by occluding the binding of A to the DNA. The rate of transcription is proportional to the probability f that the promoter is occupied. Assuming that the only factor that interacts with the polymerase is A (which in turn competes with B for DNA-binding), f will be a function only of the concentrations A and B and of the RNA polymerase concentration P. Assuming further that these molecules are in equilibrium with the DNA we may write

$$f = \frac{W_{\text{on}}}{W_{\text{on}} + W_{\text{off}}} \approx \frac{W_{\text{on}}}{W_{\text{off}}} \tag{7}$$

where

$$W_{\text{off}} = \sum_{\sigma_A, \sigma_B} W(\sigma_A, \sigma_B, 0) \tag{8}$$

$$W_{\text{on}} = \sum_{\sigma_A, \sigma_B} W(\sigma_A, \sigma_B, 1). \tag{9}$$

The statistical weights are given by

$$W(\sigma_A, \sigma_B, \sigma_P) = \omega_{AP}^{\sigma_A \sigma_P} q_A^{\sigma_A} q_B^{\sigma_B} q_P^{\sigma_P} \tag{10}$$

where $\sigma_i = 0$ if molecule i does not occupy its binding site and $\sigma_i = 1$ if it does. The statistical weights for the $(1, 1, 0)$ and $(1, 1, 1)$ configurations are zero, as configurations in which both A and B are bound to the DNA are excluded by the fact that their binding sites overlap. The cooperativity factor $\omega_{AP} \geqslant 1$ between transcription factor A and the RNA polymerase P is related to their interaction energy by $\omega_{AP} = \exp(-E_{\text{int}}/RT)$ [19]. Note that no effective interaction, $E_{\text{int}} = 0$, corresponds to a cooperativity factor of unity as is the case between B and P. The q parameters are ratios of concentrations to dissociation constants associated with binding to the DNA

$$q_X = [X]/K_X. \tag{11}$$

The statistical weights are

$$W_{\text{off}} = 1 + q_A + q_B \tag{12}$$

$$W_{\text{on}} = q_P(1 + \omega_{AP} q_A + q_B). \tag{13}$$

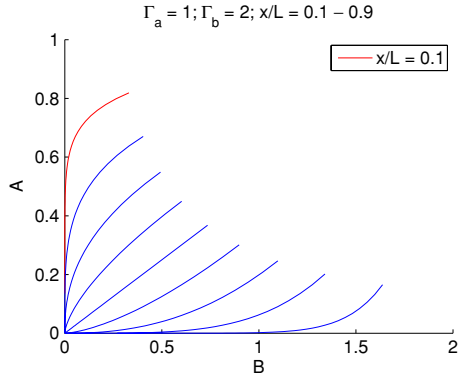

Figure 2. A plot of A against B when L is varied from 2 to 20, for different values of the scaled coordinate $\overline{x} = x/L$. The value of $\overline{x}$ ranges in steps of 0.1 from 0.1 (upper most curve) to 0.9 (lower most curve). The spatial distributions of the concentrations $A(x)$ and $B(x)$ are exponential. For the combinatorial model considered in the text the fold change in gene expression depends only on the ratio of morphogen concentrations $F(A, B) = F(A/B)$, and the expression boundary is therefore defined by a straight line (with slope r) going through the origin in the A–B plane. Scaling therefore occurs when the ratio of morphogen concentrations $A(\overline{x})/B(\overline{x})$ remains constant as L is varied. The figure shows that exponential morphogen gradients keep the ratio A/B constant only at $\overline{x} = \lambda_a/(\lambda_a + \lambda_b) = 0.5$ when L is varied. Hence perfect scaling is achieved only at the centre of the developing field when $\lambda_a = \lambda_b$, even when the source fluxes are unequal. All parameters are unity unless otherwise stated.

Inserting these weights into (7) and taking the limits $q_A, q_B \gg 1$ we obtain

$$f(A, B) \approx q_P \frac{1 + \omega_{AP} \frac{A/B}{K_a/K_b}}{1 + \frac{A/B}{K_a/K_b}} = f(A/B). \tag{14}$$

As the basal transcription rate is independent of the concentrations of A and B, the fold change $F(A, B) = f/f_0$ also depends on A and B only through their ratio, $F(A, B) = F(A/B)$. The contours of the fold change in the A–B plane are therefore straight lines going through the origin. Furthermore the position of the half-maximal contour is given by $A/B = r = K_a/K_b$.

We next define the equations governing the morphogen gradients

$$0 = D_a \partial_x^2 A - \beta_a A \tag{15}$$

$$0 = D_b \partial_x^2 B - \beta_b B \tag{16}$$

in steady state. The boundary conditions are

$$\begin{aligned} -D_a \partial_x A(0) &= \Gamma_a, & -D_a \partial_x A(L) &= 0 \\ -D_b \partial_x B(0) &= 0, & -D_b \partial_x B(L) &= -\Gamma_b. \end{aligned} \tag{17}$$

Just as in the one-gradient case, one can distinguish between relatively small systems (for which the no-flux boundary conditions matter) and large systems, depending on how big L is compared to the decay lengths λ_i. For sufficiently large L, the gradients of A and B are purely exponential, $A = A(0)\exp(-x/\lambda_a)$ and $B = B(L)\exp(-(L - x)/\lambda_b)$, where the amplitudes are given by $A(0) = \Gamma_a\lambda_a/D_a$ and $B(L) = \Gamma_b\lambda_b/D_b$. The parametric curves $(A(\overline{x}, L), B(\overline{x}, L))$ for this distribution of morphogens are shown in figure 2. One sees immediately that there is only one (straight line) parametric curve such that A/B is a constant independent of L. Hence, in principle, a pair of exponentially distributed morphogens coupled with the cis-regulatory architecture described above can set markers scale-invariantly at only one location $\overline{x}_*$ in the developing field. It is easy to show that the ratio A/B is independent of L if the normalized coordinate $\overline{x}$ is chosen to be

$$\overline{x}_* = \frac{\lambda_a}{\lambda_a + \lambda_b}. \tag{18}$$

Correspondingly the slope of the straight-line parametric curve is $A(0)/B(L)$. Therefore the ratio r of dissociation constants in the regulatory region must be

$$r_* = A(0)/B(L) \tag{19}$$

in order to obtain scaling.

Another way to obtain the parameters $\overline{x}_*$ and r_* is via the equation

$$A(\overline{x}_r, L) = rB(\overline{x}_r, L) \tag{20}$$

which defines the half-maximal contour of the fold-change function $F(A, B)$. Substituting the exponential forms for A and B we obtain

$$\overline{x}_r = \frac{\lambda_a}{\lambda_a + \lambda_b}\left\{1 - \frac{\lambda_b}{L}\ln\left(\frac{rB(L)}{A(0)}\right)\right\}, \tag{21}$$

as noted by Houchmandzadeh *et al* [17]. A number of features of this equation are worthy of note. One sees immediately that the scaled coordinate $\overline{x}_r$ reduces to the L-independent value $\overline{x}_*$ when r is put equal to r_* in agreement with the argument presented above. This is because the length scale

$$L_c(r) = \lambda_b\left|\ln\left(\frac{rB(L)}{A(0)}\right)\right| \tag{22}$$

vanishes when $r = r_*$. Equation (21) also tells us however that the scaled coordinate $\overline{x}_r$ is approximately independent of system size L even when r is not exactly r_*. More precisely, the scaled coordinate approaches $\overline{x}_*$ in the large-L limit $L_c(r)/L \ll 1$.

Hence a pair of exponential morphogen gradients whose target gene contains overlapping transcription-factor binding sites can set the gene's expression boundary at the scaled position $\overline{x}_*$ for a range of r values satisfying the inequality $L_c(r)/L \ll 1$. We note here that the scaled position $\overline{x}_*$ is (i) insensitive to source-level fluctuations, which only enter in L_c, and (ii) close to 0.5 in a system in which the degradation lengths of the two morphogen gradients are comparable.

This model can therefore achieve some degree of size-scaling near the centre of the developing field. We have in mind, however, a situation where multiple genes need to be regulated, each at different points along the developing field. We would therefore like to know how well two opposing morphogen gradients can perform in scaling a set of expression boundaries that span the developing field. Of course a pair of morphogen gradients can always be made to scale a boundary at an arbitrary location $\overline{x}$ in the developing field by choosing a cis-regulatory architecture whose half-maximal fold-change contour coincides with the $\overline{x}$ parametric curve of the gradients. Indeed, such cis-regulatory tuning of a set of genes, each

expressed in a different spatial domain but all controlled by a common pair of morphogens, may well be possible by evolution. We consider however the simpler case in which all the target genes have the simple cis-regulatory architecture described above and differ only in the value of the ratio $r = K_a/K_b$ of their dissociation constants. We then ask how well the corresponding expression boundaries can be scaled by a pair of oppositely directed morphogens.

Now each gene has its own value of r and hence its own value of $\overline{x}_r$. Equation (21) tells us how the scaled coordinate $\overline{x}_r$ changes with system size L. For those genes that satisfy $L_c(r)/L \ll 1$ the scaled coordinate depends only weakly on L. Therefore the boundaries, located close to the centre of the developing field, scale very well with system size. On the other hand for those genes that satisfy $L_c(r)/L \sim 1$ the scaled coordinate depends strongly on L. In this case, therefore, the boundaries, which are now located near the edges of the developing field, scale poorly with system size.

Equation (21) was derived using gradients that do not strictly satisfy the zero-flux boundary conditions. Therefore to quantitatively characterize the variation of $\overline{x}_r$ with L close to the edges of the developing field we must return to the expression for A in (3) (and a similar one for B). These equations lead to the following implicit equation for x_r

$$\frac{A(L)}{\cosh(x_r/\lambda_b)} = \frac{rB(0)}{\cosh((L-x_r)/\lambda_a)} \tag{23}$$

valid for a finite system. It is useful to identify what happens to x_r when the length L is made smaller. Note that there is a different behaviour depending on which of $A(L)$ and $rB(0)$ is larger. Specifically, if $A(L)$ is larger, there is a smallest length below which x_r given by this formula becomes larger than L; this length is given by

$$L^*(r) = \lambda_b \cosh^{-1}\left(\frac{A(L)}{rB(0)}\right). \tag{24}$$

If, on the other hand, the ordering is reversed, then we obtain negative values for x_r below the length scale

$$L^*(r) = \lambda_a \cosh^{-1}\left(\frac{rB(0)}{A(L)}\right). \tag{25}$$

Representative x_r/L curves are shown in figure 3 for the case of equal decay lengths $\lambda_a = \lambda_b$.

Consider now a developing field of size L subject to a natural variation in size of $L \pm pL$ with $0 \leqslant p \leqslant 1$. The variation in the fractional position at which a gene (characterized by a ratio of dissociation constants equal to r) is turned on is then given by

$$\delta\left(\frac{x_r}{L}\right) \equiv \frac{x_r(L-pL)}{L-pL} - \frac{x_r(L+pL)}{L+pL}. \tag{26}$$

We show in figure 4(a), again for the equal decay length case, the dependence of $\delta(x_r/L)$ on normalized position x_r/L in a developing field of size $L = 4$. In this figure r is an implicit parameter which is varied so that x_r/L spans the unit interval. Note that the curve terminates before the boundaries of the unit interval is reached; this is because one encounters unphysical values of $\overline{x}_r|_{L-pL}$ at these values of x_r/L. For example, the curve terminates on the right at that value of r

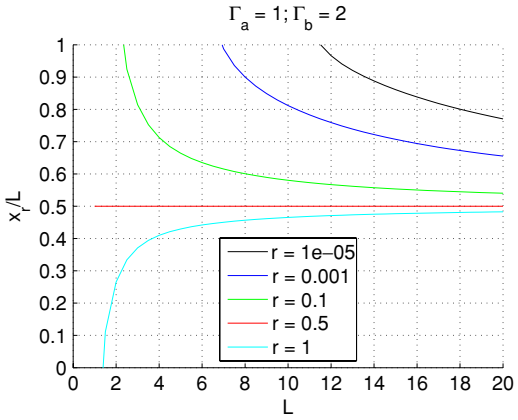

Figure 3. The combinatorial model sets markers across the developing field in a more scale-invariant fashion at larger developing field sizes L than at smaller L. This graph shows the dependence of $\overline{x}_r = x_r/L$ on system length L, as given by (23), for values of the threshold ratio equal to (from top to bottom) $r = 10^{-5}, 10^{-3}, 10^{-1}, 0.5, 1$. All parameters are unity unless otherwise stated. Note that at the position $\overline{x}_* = \lambda_a/(\lambda_a + \lambda_b) = 0.5$ the value of the ratio of dissociation constants is $r_* = A(0)/B(L) = 0.5$.

for which $\overline{x}_r|_{L-pL}$ hits unity. As expected the variation is largest (in magnitude) closest to the boundaries and vanishes at $x_r/L = \overline{x}_*$. Now define an arbitrary scaling criterion by

$$\delta(x/L) \leqslant 5\%. \tag{27}$$

Then, according to this criterion, exponentially distributed morphogen gradients coupled to a cis-regulatory architecture of the form $F(A, B) = F(A/B)$ scale expression boundaries only in the central region of the developing field between about 30% and 70% of L when $L = 4$.

Closest to the edges of the developing field the variation $\delta(x_r/L)$ is about 14%. Since the slopes of the x_r/L curves at $x_r/L = 1$ become flatter as L is increased (see figure 3), one might wonder whether operating at larger system sizes will decrease this variation. This would in turn increase the fraction of the developing field over which scaled boundaries exist. However, at larger system sizes the flattening effect is offset by the fact that one must sample larger and larger portions of the x_r/L curve when evaluating $\delta(x_r/L)$. The extent to which these effects cancel is shown in figure 4(b) where we show the variation $\delta(x_r/L)$ closest to the right boundary of the developing field as a function of L. The variation decreases with increasing L, but an elementary calculation, outlined in the appendix, reveals that it has the lower bound $p/(1+p)$. For a percentage variation $p = 10\%$ in system size this lower bound is about 9%. We conclude that increasing system size is not sufficient to make the combinatorial model, in the particular guise considered here, meet the scaling criterion in (27) throughout the developing field.

A further difficulty with the combinatorial model is its susceptibility to small-molecule-number fluctuations. In general, we must expect L_c of order λ, since we cannot independently adjust the morphogen sources for the multiple genes that need to be controlled. In fact, the natural

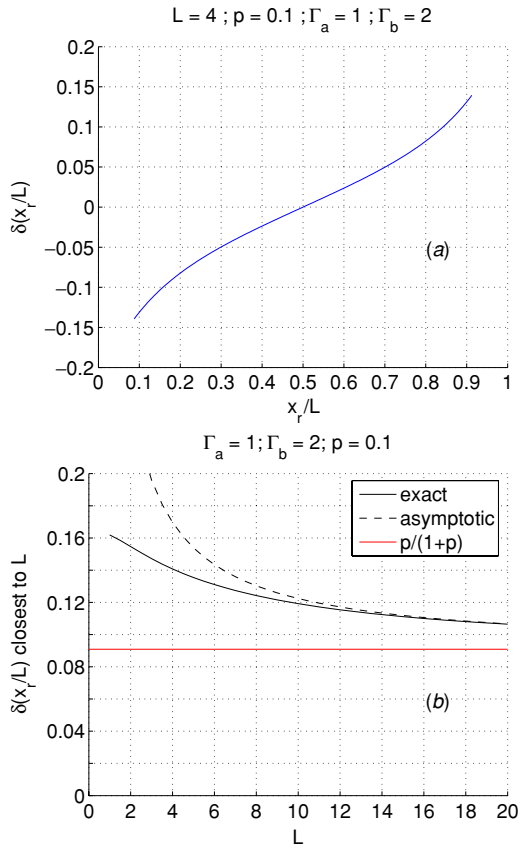

Figure 4. (*a*) Quantitative measure of the scalability of markers at various locations in the developing field in the combinatorial model showing that markers become less scalable as they move away from $\overline{x}_*$. This graph shows the variation $\delta(x_r/L)$, as defined in (26), as a function of normalized position x_r/L in the developing field for $L = 4$ and a percentage change in system size of 10%. The point at which the curve crosses zero is $\overline{x}_*$. (*b*) The variation $\delta(x_r/L)$ closest to the right boundary of the developing field as a function of L (solid line). At each L we have chosen the target gene whose threshold ratio r satisfies $L^*(r) = L - pL$. The variation in the fractional position at which this gene is turned on is then given by $\delta(\frac{x_r}{L}) = 1 - \frac{x_r(L+pL)}{L+pL}$. The dashed line is the asymptotic expression in (A.8). The horizontal (red) line is the limiting value $p/(1+p)$ of the solid and dashed curves.

interpretation of r as being due to binding differences between different transcription factors suggests that L_c would vary significantly. In such cases the limit $L \gg L_c$ would force the comparison point x_r far down the profile from the source; having enough molecules at this point to effect the necessary DNA binding would then place a severe constraint on source strengths. In more detail, a nucleus with volume V_n would see a fractional fluctuation in molecule numbers of order $(A(x_r)V_n)^{-\frac{1}{2}}$. Were this to be interpreted as a shift in the matching point, we would obtain an error

$$\delta\left(\frac{x_r}{L}\right) \simeq \frac{\lambda}{L}\frac{1}{\sqrt{A(x_r)V_n}}. \tag{28}$$

The nuclear volume is probably of order 1 μm^3; hence a 5% error at, say, $L = 8$ would necessitate a matching point concentration of approximately 10 nM. Since this is down by a factor of 10–50 from the boundary concentration, this may begin to be a serious limitation on the efficacy of the combinatorial approach. In this regard a combinatorial mode of action may favour power law (resulting e.g. from nonlinear degradation [20]) over exponential profiles, as the former have greater range than the latter. This, however, remains to be studied.

4. Annihilation model

We return to the standard model of morphogenesis in which cell-fate boundaries are determined according to the position at which a single morphogen crosses a threshold concentration. We couple this gradient to an auxiliary gradient directed from the opposite end of the developing field. We then ask under what conditions the primary gradient may scale with system size.

We consider two species of morphogen, A and B, in a one-dimensional system of length L with As and Bs injected at opposite ends of the system. The boundary conditions are as in section 3. The species interact according to the annihilation reaction $A + B \to \emptyset$. In a mean-field description the kinetics is described by the reaction–diffusion equations

$$\partial_t A = D_a\partial_x^2 A - \beta_a A - kAB \tag{29}$$

$$\partial_t B = D_b\partial_x^2 B - \beta_b B - kAB \tag{30}$$

where k is the annihilation rate constant. Later, we will consider more complex models which incorporate nonlinear degradation or nonlinear (i.e. concentration-dependent) diffusion.

This system of equations, with fluxes $\Gamma_a = \Gamma_b = \Gamma$ and without any proteolysis ($\beta_a = \beta_b = 0$), was considered by Ben-Naim and Redner [21]. They determined the steady-state spatial distribution of the reactants and of the annihilation zone which they chose to be centred in the interval $[0, L]$. The annihilation zone is roughly the support of $R(x) = kA(x)B(x)$ or, put another way, that region where the concentration of both species is appreciable. With the aid of a rate-balance argument, they showed that the width w of the annihilation zone scales as $\Gamma^{-1/3}$ and that the concentration in this zone is proportional to $\Gamma^{2/3}$ when $w \ll L$.

Our goal is to understand the relation of the steady-state concentration profiles to the system length L. It is convenient to identify the point x_e in the annihilation zone where the profiles cross, $A(x_e) = B(x_e)$. In the original Ben-Naim–Redner model, the reaction–diffusion equations yield no unique value for x_e; instead x_e can lie anywhere in the interval $[0, L]$ depending on the choice of initial condition. To see this consider the following rate-balance argument. Since the particles annihilate in a one-to-one fashion the flux of each species into the annihilation zone must be equal. But this condition does not determine x_e uniquely because these fluxes are always equal to the input fluxes at the boundaries. Similarly, the model without proteolysis cannot support steady states with unequal boundary fluxes. If, however, we now add active degradation terms to the steady-state equations, then the flux of each species into the annihilation zone is the flux into

the system less the number of degradation events that happen before reaching the zone. Thus, the flux of each species into the annihilation zone now depends on the location x_e and so there is only one value of x_e that balances the fluxes. As we will see, our models will always contain unique steady-state solutions.

A rough estimate of the concentration in the annihilation zone and of the width of the zone can be obtained using the original Ben-Naim–Redner rate-balance argument [21]. We identify three spatial regions: the first where A is in the majority; the second the annihilation zone; and the third where A is in the minority. Assume that the concentration of As in this latter region is negligible compared with that in the other two regions. The concentration of As in the annihilation zone should then be on the order of the slope of the concentration profile in the annihilation zone times the width w. The slope of the A profile in this region is proportional to j_e/D_a, where j_e is the equal flux of As or Bs into the annihilation zone. Therefore the concentration in the annihilation zone $A_e = A(x_e)$ is

$$A_e \sim j_e w/D_a. \tag{31}$$

If we ignore the loss of A particles in the annihilation zone due to proteolysis (a valid approximation for small enough w), then the number of annihilation events per unit time $kA_e^2 w$ should equal the flux j_e. Balancing these two rates gives $j_e \sim k(j_e w/D_a)^2 w$. Hence the width of the annihilation zone scales as

$$w \sim \left(\frac{D_a^2}{j_e k}\right)^{1/3}. \tag{32}$$

In what follows, we will be mostly interested in taking k large enough to give a very small w.

5. The high-annihilation-rate limit

We now explicitly assume that the parameters lie in the limit where $w \ll \min\{x_e, L - x_e\}$. This limit has the considerable advantage that the A–B system may be decoupled by replacing the coupling term kAB by a zero-concentration boundary condition at x_e. In this approximation the concentration of the A subsystem satisfies

$$0 = D_a \partial_x^2 A - \beta_a A \tag{33}$$

subject to the boundary conditions $-D_a \partial_x A(0) = \Gamma_a$ and $A(x_e) = 0$. The solution to this equation is

$$A(x) = \frac{\lambda_a \Gamma_a}{D_a \cosh(x_e/\lambda_a)} \sinh\left(\frac{x_e - x}{\lambda_a}\right) = A_* \sinh\left(\frac{x_e - x}{\lambda_a}\right) \tag{34}$$

where as before $\lambda_a = \sqrt{D_a/\beta_a}$. A_* is a characteristic concentration of the A field related to the slope of the A field at x_e according to $A_* = -\lambda_a \partial_x A(x_e)$. The flux of A particles is

$$j_a(x) = j_a(x_e) \cosh\left(\frac{x_e - x}{\lambda_a}\right) \tag{35}$$

where the flux into the annihilation zone $j_a(x_e)$ is given by $j_a(x_e) = \Gamma_a/\cosh(x_e/\lambda_a)$. Substituting this into (32) yields the scaling function of the annihilation zone width for the case of linear degradation

$$w \sim w_0 \left[\cosh(x_e/\lambda_a)\right]^{1/3}. \tag{36}$$

Here $w_0 \sim \left(D_a^2/\Gamma_a k\right)^{1/3}$ is the width of the annihilation zone in the absence of degradation [21]. Note that we may also substitute this expression for $j_a(x_e)$ into (31) obtaining $A_e \sim w/\cosh(x_e/\lambda_a)$. One can then verify that A_e is much smaller than $A(0)$ whenever $w \ll x_e$ and hence approximating this as a zero boundary condition is self-consistently valid.

The B subsystem can be treated similarly, except that the length of the subsystem in this case is $L - x_e$. The only dependence on the annihilation rate k in the inequality $w \ll x_e$ occurs in w_0. Hence this limit is equivalent to the high-annihilation-rate limit $k \gg k_0$, where the threshold value k_0 of the annihilation rate is given by

$$k_0 \sim \frac{D_a^2}{\Gamma_a \lambda_a^3} \frac{\cosh(x_e/\lambda_a)}{(x_e/\lambda_a)^3}. \tag{37}$$

We determine the annihilation zone location by balancing fluxes into the zone, $j_a(x_e) = -j_b(L - x_e)$. This leads to the following equation for x_e:

$$\frac{\Gamma_a}{\cosh\left(\frac{x_e}{\lambda_a}\right)} = \frac{\Gamma_b}{\cosh\left(\frac{L - x_e}{\lambda_b}\right)}. \tag{38}$$

In the special case $\lambda_a = \lambda_b$ this equation coincides with the implicit definition of x_r (with $r = 1$) which arose in the combinatorial model (see (23)). As in that model there is a smallest length L^* defined by

$$L^* = \lambda_a \cosh^{-1}\left(\frac{\Gamma_a}{\Gamma_b}\right)$$

if $\Gamma_a > \Gamma_b$ and by

$$L^* = \lambda_b \cosh^{-1}\left(\frac{\Gamma_b}{\Gamma_a}\right)$$

if the flux ordering is reversed. As our entire treatment of the annihilation zone only makes sense if $0 \leqslant x_e \leqslant L$, we must always choose $L \geqslant L^*$. A comparison of the numerical solution of the full model with the results of the large-annihilation-rate approximation is shown in figure 5.

Once we know $x_e(L)$ and $A(x)$, we can proceed to determine the qualitative features of the $x_t(L)$ function with a view to identifying the region of system sizes where $x_t \sim L$. Inverting (34) we find

$$x_t = x_e - \lambda_a \sinh^{-1} \eta \tag{39}$$

where

$$\eta = A_t/A_*. \tag{40}$$

Note that x_t depends on L only through its dependence on x_e and the function $x_t(x_e)$ is monotonically increasing. Obviously $x_t \leqslant x_e$. In the limit of sufficiently large x_e, we can replace the inverse hyperbolic function with a logarithm and obtain the simpler form

$$x_t \approx x_e - \lambda_a \ln(2\eta). \tag{41}$$

Here, $\eta \approx \frac{A_t}{A(0)} \frac{1}{2} e^{x_e/\lambda_a}$, and x_t approaches its asymptotic value $x_\infty \approx \lambda_a \ln(A(0)/A_t)$ from below. This is of course the

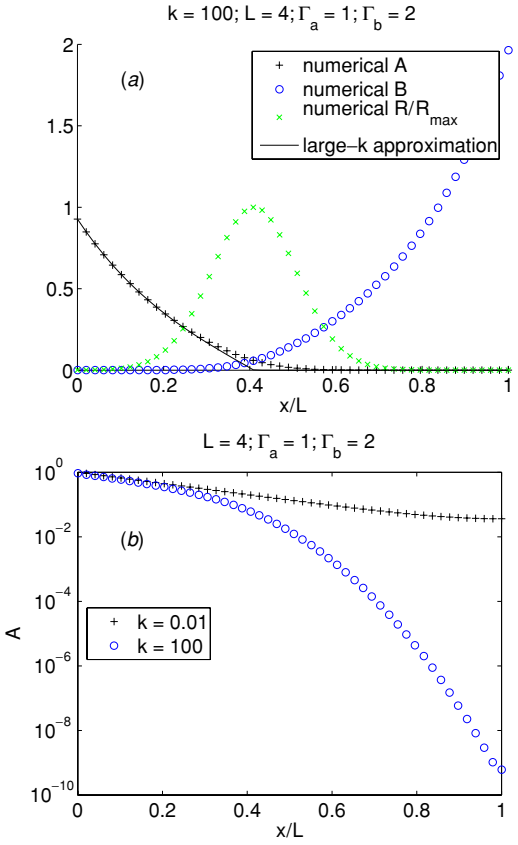

Figure 5. (*a*) The high-annihilation-rate approximation is quite accurate at $k = 100$. Here this approximation (solid line, see (34)) is compared with the numerical solution (plus signs) of the full annihilation model (see (29) and (30)). The annihilation zone is the reaction front $R(x) = kA(x)B(x)$. All parameters are unity unless otherwise stated. (*b*) $A(x)$ plotted on a logarithmic scale in the cases $k = 0.01$ and $k = 100$. Note the crossover from slow decay in the A-rich region to fast decay in the B-rich region in the case $k = 100$. All parameters are unity unless otherwise stated.

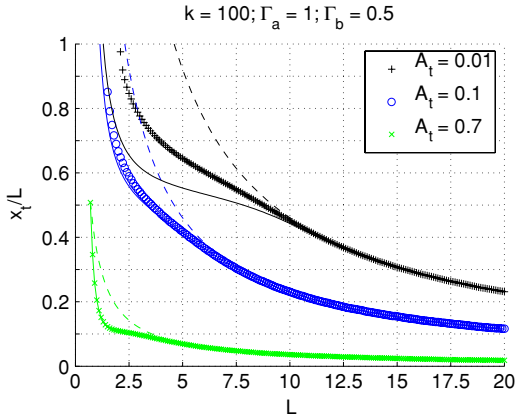

Figure 6. The annihilation model does not show a scaling region when the A flux is greater than the B flux. Dependence of normalized x_t on system length L with $k = 100$ and $\Gamma_b < \Gamma_a$. The plus signs, circles and crosses are numerical solutions of equations (29) and (30) for values of the threshold concentration equal to (from top to bottom) $A_t = 0.01, 0.1, 0.7$. The solid lines are the corresponding analytic expressions (39) obtained in the high-annihilation-rate limit. Dashed lines are x_∞/L curves as given by (6). All parameters are unity unless otherwise stated.

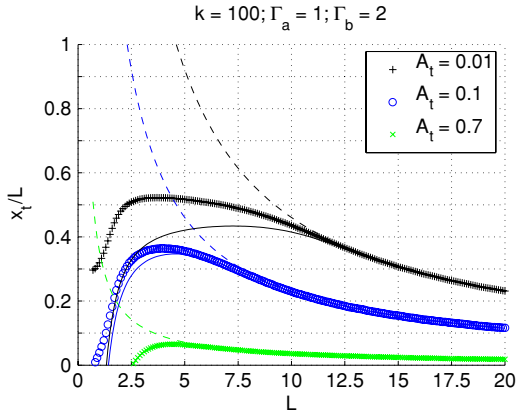

Figure 7. The annihilation model can set markers across half of the developing field ($L \approx 4$) in a roughly scale invariant manner when the A flux is less than the B flux. Dependence of normalized x_t on system length L with $k = 100$ and $\Gamma_b > \Gamma_a$. The plus signs, circles and crosses are numerical solutions of equations (29) and (30) for values of the threshold concentration equal to (from top to bottom) $A_t = 0.01, 0.1, 0.7$. The solid lines are the corresponding analytic expressions (39) obtained in the high-annihilation-rate limit. Dashed lines are x_∞/L curves as given by (6). All parameters are unity unless otherwise stated.

answer one would obtain in the absence of any auxiliary gradient.

Now, imagine reducing L and hence x_e from its just-mentioned asymptotic regime and plotting the ratio x_t/L. For the case $\Gamma_a > \Gamma_b$, x_e will eventually hit L followed shortly thereafter by x_t/L hitting unity. There is no reason why this curve should exhibit a maximum, and a direct numerical calculation for $k = 100$ (shown in figure 6) verifies this assertion. The situation is dramatically different, however, for the case of $\Gamma_b > \Gamma_a$. Now x_e must approach zero, implying that at some larger L we have $x_t = 0$. The curve x_t/L now exhibits a maximum, as is again verified by direct numerical calculations using both the large-annihilation-rate approximation and also by just solving the initial model with no approximations whatsoever (see figure 7). Near the peak of the curve we have scaling with system size. For completeness, we also present in figure 8 the results for equal fluxes.

To compare the scaling performance of the annihilation model with that of the combinatorial model we show in figure 9 the dependence of the variation $\delta\,(x_t/L)$ on normalized position x_t/L in the developing field for $L = 4$. One sees that, according to our scaling criterion in (27), the annihilation mechanism can easily set markers scale-invariantly throughout a developing field whose size is a few decay lengths. Furthermore at such system sizes a range of threshold values spanning two orders of magnitude ($c_t = 0.01$–0.7) is sufficient to cover the entire developing field (see the $k = 100$ results in figure 7). Such a modest variation in concentration makes the annihilation model less susceptible

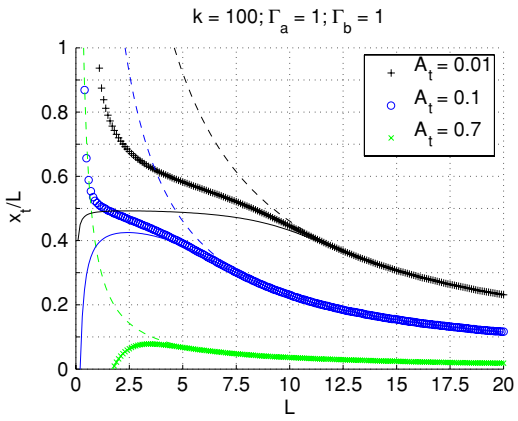

Figure 8. When the A and B fluxes are equal only some of the x_t/L curves have maximums as a function of L. Dependence of normalized x_t on system length L with $k = 100$ and $\Gamma_b = \Gamma_a$. The plus signs, circles and crosses are numerical solutions of equations (29) and (30) for values of the threshold concentration equal to (from top to bottom) $A_t = 0.01, 0.1, 0.7$. The solid lines are the corresponding analytic expressions (39) obtained in the high-annihilation-rate limit. Dashed lines are x_∞/L curves as given by (6). All parameters are unity unless otherwise stated.

to small-molecule-number fluctuations than the combinatorial model.

6. Discussion

We have considered two scenarios in which a pair of oppositely directed morphogen gradients are used to set embryonic markers in a size-invariant manner. In the simplest scenario, in which the gradients interact only indirectly through overlapping DNA-binding sites, exponentially distributed fields achieve perfect size scaling at a normalized position $\lambda_a/(\lambda_a+\lambda_b)$ determined only by the morphogen decay lengths λ_a and λ_b. For equal decay lengths, the accuracy with which this model can set markers size-invariantly decreases as the boundaries of the developing field are approached. At the boundaries the accuracy can be no better than $\delta(x_r/L) = p/(1+p)$ where p is the percentage variation of the field size. In the second model A and B are coupled via the reaction $A + B \to \emptyset$ and the embryonic markers are set by a single gradient with the second gradient serving only to provide size information to the first. In this scenario, it is easy to arrange parameters such that scaling occurs with an accuracy, measured by $\delta(x_t/L)$, of better than 5% over the entire developing field for field sizes of only a few decay lengths.

In practice a given morphogen may play both roles in patterning, setting markers in a strictly concentration-dependent manner at some locations in the developing field and in a combinatorial fashion at other locations [13]. The annihilation model naturally sets markers via the gradient whose source is closest to the marker [22], whereas the combinatorial model is better suited to setting markers in the vicinity of the midpoint of the developing field where the variation $\delta(x_r/L)$ is smallest. As the variation $\delta(x/L)$ has

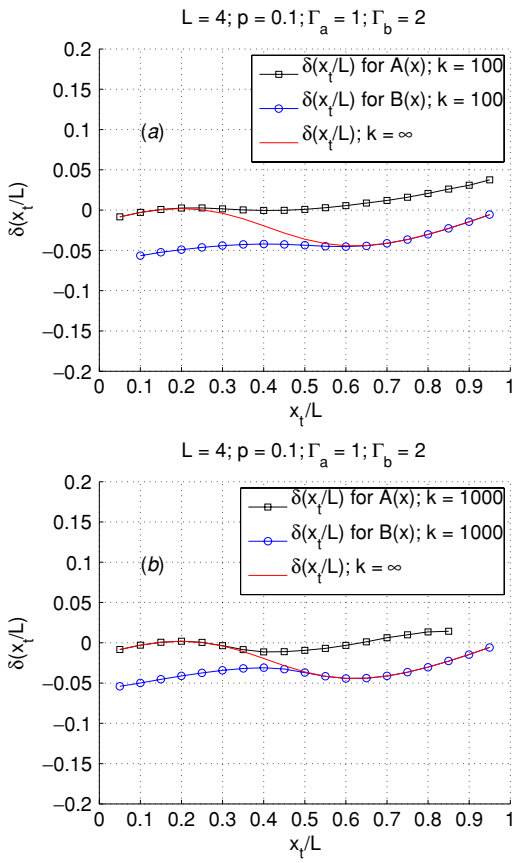

Figure 9. According to the scaling criterion $\delta(x/L) \leqslant 5\%$ the annihilation mechanism can set markers scale-invariantly throughout a developing field whose size is a few decay lengths. Both graphs above show the dependence of the variation $\delta(x_t/L)$ on normalized position x_t/L in the high-annihilation-rate approximation of the annihilation model (solid red lines). Positions to the left of $x_e/L \approx 0.4$ are set by the A gradient while positions to the right are set by the B gradient (see figure 5). In addition we show the dependence of $\delta(x_t/L)$ on x_t/L for (*a*) $k = 100$ and (*b*) $k = 1000$. All parameters are unity unless otherwise stated.

a qualitatively different dependence on x/L in either case, a measurement of this curve in a developmental system may distinguish between the mechanisms.

The origin of the scaling form $f(x/L)$ which arises in the strong-coupling limit of the annihilation model is the effective boundary condition $A(x_e) = 0$. In the case $\Gamma_b > \Gamma_a$ (see figure 7) the x_t/L curve has a maximum because at small L ($L \sim L_*$) it tends to zero along with x_e/L while at large L ($L \gg L_*$) it is bounded above by x_∞/L. In the $k \ll k_0$ limit, on the other hand, the zero-concentration effective boundary condition is replaced by a zero-flux boundary condition $j_a(L) = 0$ which can never induce the $x_t \sim L$ scaling.

This approach makes it clear why the scaling occurs at intermediate values of L. Once we reach the non-overlapping limit where the two fields do not effectively communicate, the threshold is set by the A profile alone; we have already seen that this cannot give any scaling. For L too small, the annihilation-zone width w becomes comparable to x_e, there

is no effective boundary condition and again scaling fails. In fact, if one looks at the expression for w/x_e, namely

$$\frac{w}{x_e} \sim \frac{w_0}{\lambda_a}\left(\frac{\cosh(x_e/\lambda_a)}{(x_e/\lambda_a)^3}\right)^{1/3} \tag{42}$$

(where $w_0 \sim \left(D_a^2/\Gamma_a k\right)^{1/3}$), one sees that the maximum in x_t/L occurs close to the minimum of w/x_e which is reached at $x_e/\lambda_a \approx 3$.

So far we have used linear degradation and simple diffusion in the annihilation model. However, it should be clear from the arguments above that the qualitative features of this model are rather insensitive to changes in the nature of the individual gradients. As an example, let us consider quadratic degradation. In the limit that the system size is so big as to render the coupling term kAB irrelevant, the A and B profiles reduce to power laws, $A = a/(x+\epsilon_a)^2$ and $B = b/(L-x+\epsilon_b)^2$. The corresponding L-independent threshold position x_∞ is given by

$$x_\infty = \epsilon_a\left(\sqrt{\frac{A(0)}{A_t}} - 1\right). \tag{43}$$

An argument similar to one presented earlier for linear degradation shows that as L is decreased from this large-L limit, x_e will eventually be forced to zero provided $\Gamma_b > \Gamma_a$. This indicates again that, to the extent we can believe the large-annihilation-rate approximation, there will be a maximum in the x_t/L curve. This is illustrated for one specific choice of parameters in figure 10(*a*). The maximum again takes place roughly where L becomes so small as to cause the annihilation-zone width to approach x_e. Repeating the derivation of w outlined in section 5 but using a power law for $A(x)$ instead of hyperbolic sine we obtain

$$\frac{w}{x_e} \sim \frac{w_0}{\epsilon_a}\left(1 + \frac{1}{x_e/\epsilon_a}\right). \tag{44}$$

This expression is a good qualitative description of the exact w/x_e shown in figure 10(*a*) and diverges when $L \to 0$ as in the case of linear degradation. Note that scaling is lost when $w \to x_e$ even though the rate of the annihilation reaction becomes large (figure 10(*b*)). Finally, one can also ask about the effect of making the diffusion constant concentration dependent. This type of effect can arise whenever the morphogen reversibly binds to buffers that differ in mobility from the pure molecule. Figure 11 illustrates the behaviour under the simplest assumption, namely that the diffusion constant varies linearly with concentration for both the A and B fields. Aside from sharpening the transition from the asymptotic non-interacting regime to the regime where x_e approaches zero (as L is lowered), the basic phenomenology is unchanged.

The focus of our work has been the scaling issue. However, we should not lose track of the other requirement for developmental dynamics, namely that the system be relatively robust to fluctuations in parameters such as source fluxes. Figure 12(*a*) presents data regarding the variation of x_t with Γ_a and Γ_b in the annihilation model. For simplicity the data are presented for the case of equal decay lengths, $\lambda_a = \lambda_b = \lambda$.

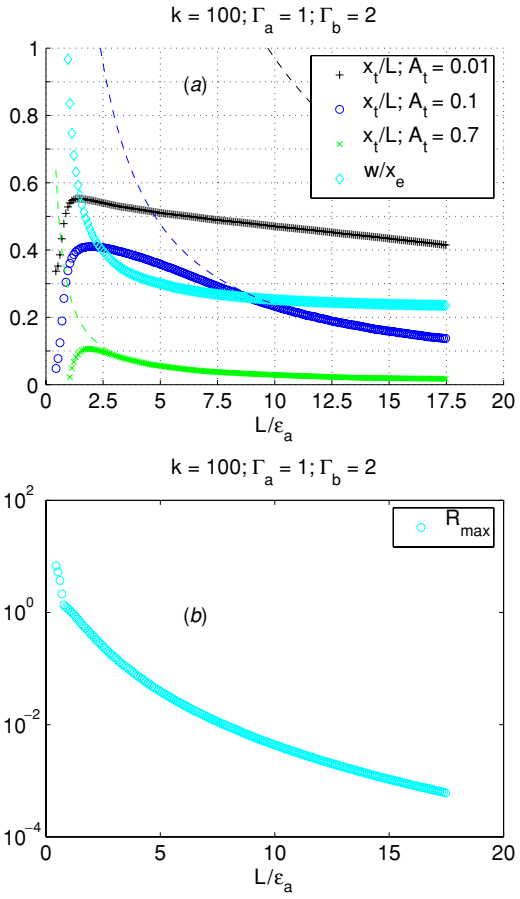

Figure 10. (*a*) Quadratic degradation does not alter the qualitative form of the x_t/L curves in the annihilation model. The plus signs, circles and crosses are numerical solutions of the full annihilation model for values of the threshold concentration equal to (from top to bottom) $A_t = 0.01, 0.1, 0.7$. The dashed lines are x_∞/L curves as given by (43). Also shown (cyan diamonds) is the ratio of the full width at half maximum w to the comparison point x_e. (*b*) The dependence of the amplitude $R_{\max}$ of the local annihilation rate $R(x) = kA(x)B(x)$ on system length L. In (*a*) and (*b*) all parameters are unity unless otherwise stated.

The basic conclusion is that the coefficient of variation χ_i, defined as

$$\frac{\delta x_t}{\lambda} = \begin{cases} \chi_a \frac{\delta\Gamma_a}{\Gamma_a} \\ -\chi_b \frac{\delta\Gamma_b}{\Gamma_b}, \end{cases} \tag{45}$$

starts at $1/2$ at $A_t = 0$ and then asymptotes to either 1 for variations in Γ_a or zero for variations in Γ_b. These asymptotic values are of course precisely the results obtained for the one-exponential-gradient model. The fact that χ_i at small x_t is $1/2$ can be understood by noting that in this limit x_t is just x_e, which can easily be shown to be approximately (i.e. for large enough L) $x_e \approx 0.5(L \pm L_c)$ with $L_c = \lambda\,|\ln(\Gamma_b/\Gamma_a)|$. With this approximation for x_e and taking differentials of x_t we obtain

$$\chi_a = \frac{1}{2} + \frac{\eta}{\sqrt{1+\eta^2}}\left[1 - \frac{1}{2}\tanh\left(\frac{x_e}{\lambda}\right)\right] \tag{46}$$

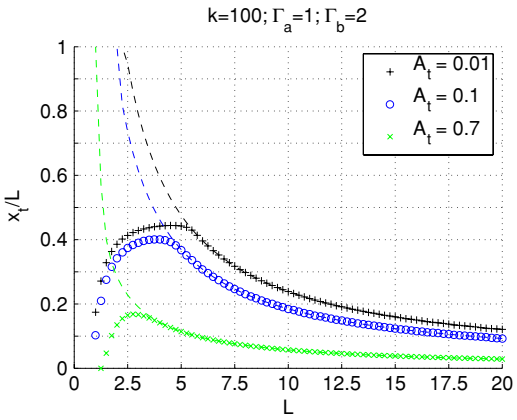

Figure 11. The qualitative form of the x_t/L curves is not affected by the addition of nonlinear diffusion to the annihilation model. The graph shows the dependence of scaled threshold position x_t/L on system length L in the simplest case of nonlinear diffusion, $D_a = \delta_a A$ and $D_b = \delta_b B$. The degradation terms are linear. The plus signs, circles and crosses are numerical solutions of the full annihilation model for values of the threshold concentration equal to (from top to bottom) $A_t = 0.01, 0.1, 0.7$. Dashed lines are corresponding curves in the case $k = 0.01$. All parameters are unity unless otherwise stated.

$$\chi_b = \frac{1}{2}\left[1 - \frac{\eta}{\sqrt{1+\eta^2}}\tanh\left(\frac{x_e}{\lambda}\right)\right] \tag{47}$$

where, as before, $\eta = A_t/A_*$. These are good approximations at all values of η for percentage variations in source fluxes as large as 5% (see figure 12(a)). The reduction of the χ values from unity represents an increase in system robustness as compared with the single-exponential-gradient model (albeit with a new sensitivity to the B gradient) in agreement with earlier work [16]. For comparison we also show in figure 12(b) the coefficient of variation that arises in the single-gradient model. The approximation to χ_a in this case is given by

$$\chi_a = \frac{\eta}{\sqrt{\eta^2 - 1}} \tag{48}$$

where now η is defined by $\eta = A_t/A(L)$. Note that the effect of the boundary ($\eta \downarrow 1$) is to increase the sensitivity of the gradient to variations in the source flux over that for a simple exponential.

The coefficient of variation χ_i in the combinatorial model is also smaller than unity [17]. However, Howard and ten Wolde, who considered both correlated and uncorrelated fluctuations in the A and B sources, have found that a combinatorial mechanism is less robust to variations in its parameters than an annihilation mechanism [16].

The *bicoid-hunchback* system is an ideal platform to test the ideas explored in this work. The embryo at this stage of development is a quasi-two-dimensional array of nuclei in a common cytoplasm and the diffusive properties of the Bicoid morphogen in the syncytium have recently been characterized [9]. In addition the Bicoid-DNA dissociation constant is known and is approximately $K_D \sim 10$ nM to 100 nM [23]. However, more quantitative work needs to be done. The

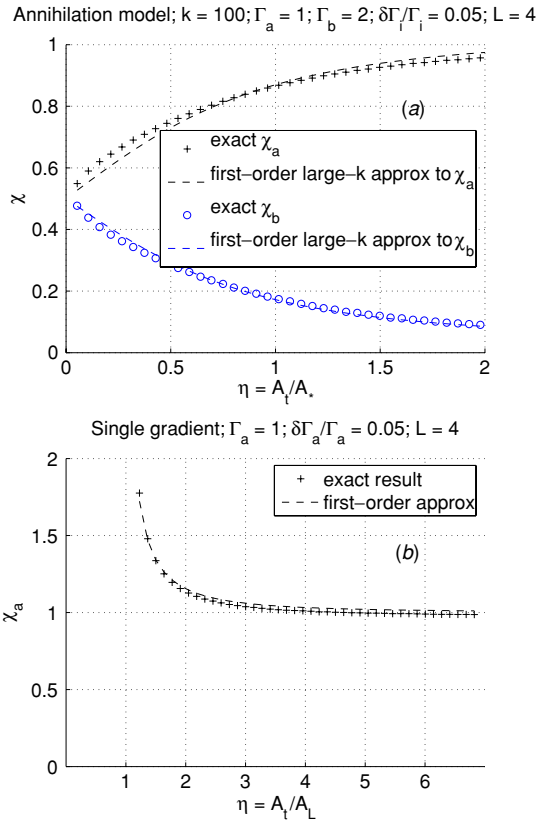

Figure 12. Simple quantitative measure of the robustness of (a) the annihilation mechanism and (b) the single-source model to source-level fluctuations. Shown are sensitivity of the threshold position x_t to infinitesimal variations in the source fluxes Γ_a and Γ_b in (a) the annihilation model (constant diffusion constant and linear degradation) and (b) the single-gradient model. The coefficient of variation χ_i is defined by (45) in the text. The data plotted as plus signs and circles were obtained by solving numerically the full model, while the dashed lines represent (from top to bottom) equations (46), (47) and (48). All parameters are unity unless otherwise stated.

concentration of Bicoid and Hunchback protein in the embryo are not known, though the intraembryonic concentration of the Pumilio protein, a translational regulator of the *hunchback* gene in *Drosophila*, has been estimated to be about 40 nM [24]. It is also crucial to measure the flux of Bicoid being translated at the anterior end of the embryo. Finally, it is not yet known when precisely the Bicoid gradient is actually read [11], although we have assumed here that the gradient reaches steady state before it begins transcription.

A large-scale search of the *Drosophila* genome uncovered only one gene that affected precision [2, 25]. This gene, a maternal gene called *staufen*, creates a product that is known to localize to both poles of the egg [26, 27], suggestive of the existence of two opposing gradients. There is however no direct evidence for a second gradient opposing the maternal Bicoid gradient, though the Bicoid protein does contain domains by which co-repressors affect its activity [28] as recently pointed out by Howard and ten Wolde [16]. In this regard, it is worth recalling that the annihilation mechanism relies on the existence of an active form of the Bicoid protein

A, and an inactive form A_* in which A is bound to a co-repressor. It may be the case that current experiments have probed only the total Bicoid concentration $A(x) + A_*(x)$, and not the active gradient $A(x)$. An immunostaining experiment designed to discriminate between the active and inactive forms of A (possibly by directing the antibody to bind one or more of Bicoid's repression domains) would offer a definitive test of the annihilation mechanism in the *bicoid-hunchback* problem; this has not yet been investigated. In principle one can also determine the spatial distribution of the complex A_* by fluorescence resonance energy transfer. Thus, at least for the time being and for this particular system, our proposed scaling mechanism must be considered to be conjectural. Moreover, although a cancellation of effects [17] can in principle explain the two-temperature microfluidics experiment of Lucchetta *et al* on the *Drosophila* embryo [18], the ability of developmental patterning to compensate for a temperature gradient remains challenging to explain with a two-gradient hypothesis.

In terms of applying our general results to the specific case of Bicoid, we should also mention the very recent re-examination by Crauk and Dostatni of the *hunchback* scaling problem [25]. The authors looked at mRNA distributions instead of protein distributions [2] confirming that the pattern scaling phenomenon occurs at the level of transcription. They showed that a lacZ reporter gene, with only Bicoid binding sites upstream of the transcription start site, also produced a scaled expression profile. This calls into question the applicability of a combinatorial model to scaling in this system. Surprisingly, Crauk and Dostatni also showed that Gal4-derived transcription factors, when expressed in a Bicoid-like gradient in the embryo, can also scale the expression pattern of a Gal4-responsive transgene. Bicoid and Gal4-3GCN4 (one of the transcription factors used) have no sequence homologies. But the annihilation mechanism relies on the ability of an activator to bind to another molecule (termed a co-factor) that inhibits its transcriptional activity. If we are to believe the annihilation mechanism, Crauk and Dostatni's work shows that this co-factor must act generally enough to interact with both Bicoid and Gal4-3GCN4. Alternatively, scaling must work by modulating the mRNA localization by some unknown mechanism and would hence fall outside the considerations of this paper.

With a scaling criterion $\delta(x/L) < 5\%$, the annihilation model predicts that the embryo can tolerate a variation in L/λ about the value $L/\lambda \approx 4 - 5$ of no more than about 20%. The embryo can therefore buffer small variations in L, which arise from embryo variability within a species, without adjusting λ. Within the annihilation framework however larger changes in L must be accompanied by a proportionate change in λ if the embryo is to continue to buffer small embryo-to-embryo variability in L. Large changes in L can occur across species where, for example, the eggs of closely related dipteran species vary over at least a factor of 5 in length. The proportionality of λ with L that emerges in the annihilation model is supported by recent experiments on embryos of a number of dipteran species [9].

7. Conclusion and outlook

In this paper, we have shown that coupling two oppositely directed morphogen gradients allows patterns to be set in approximate proportion to the size of the developing field. We have considered two coupling mechanisms, the most effective of which couples the gradients via a phenomenological annihilation reaction. Such a mechanism can set boundaries of gene expression across the developing field with a small sample-to-sample variation in the normalized position of the boundaries. In this scenario, there is no magic bullet that ensures either exact scaling or complete robustness. Instead, the effective boundary condition created by the annihilation reaction allows approximate scale invariance to emerge in one reasonably-sized range of parameter space and similarly lowers the sensitivity of any threshold to source-level fluctuations. Our general framework predicts the emergence of pattern scaling at developing-field sizes of approximately four to five times the decay length. This is in good agreement with measurements in the *Drosophila* embryo [2] and provides a natural explanation for the scaling of decay length with embryo size observed recently in a number of closely related dipteran species [9]. Presumably, one could obtain even more robustness, better scaling, and possibly even temperature compensation [18], via the introduction of additional interactions.

As has been emphasized throughout, our work addresses the general question of precise scaling without committing to the specifics of any explicit example. As attractive as it might be to apply our two gradient model to the well-studied *bicoid-hunchback* problem, there are possible difficulties with this notion. We look forward to more detailed quantitative measurements of the relevant concentration profiles in this (and other systems) as we try to unravel the mechanisms used to ensure the proper patterning of growing embryos.

Acknowledgments

This work has been supported in part by the NSF-sponsored Center for Theoretical Biological Physics (grant numbers PHY-0216576 and PHY-0225630). PM acknowledges useful discussions with E Levine, T Hwa and A Eldar.

Appendix

Consider the set of x_r/L curves shown in figure 3. Each curve intersects zero or unity at a field size $L = L_*(r)$. For a given developing field size L there is a range of r values such that the corresponding x_r/L values span the unit interval. The variation

$$\delta\left(\frac{x_r}{L}\right) \equiv \frac{x_r(L - pL)}{L - pL} - \frac{x_r(L + pL)}{L + pL} \tag{A.1}$$

will in general start at zero at $x_r/L = \overline{x}_*$ and increase monotonically as the edges of the developing field are approached. We wish to find the maximum value this variation attains throughout the developing field in the limit of large field sizes. Since the curve is symmetric for $\lambda_a = \lambda_b = \lambda$ it is

sufficient to focus on the edge $x = L$. As the variation samples the x_r/L curve at $L_l = L - pL$ it is clear that at $x_r/L = 1$ the variation uses an unphysical value $x_r/L > 1$. In other words for each L there is a limit to how small we can make r while still evaluating a physically sensible variation. This limiting value of r, call it r_L, is defined by $L_*(r_L) = L_l = L - pL$ which can be rewritten as

$$r_L \Gamma_b / \Gamma_a = 1/\cosh(L_l/\lambda) \tag{A.2}$$

with the aid of (24). By definition we have

$$\delta\left(\frac{x_{r_L}}{L}\right) = 1 - \frac{x(r_L, L + pL)}{L + pL}. \tag{A.3}$$

Now when the system size is $L_u = L + pL$ the point at which $A/B = r_L$ is given by

$$x(r_L, L_u) = -\frac{\lambda}{2} \ln \gamma(r_L, L_u) \tag{A.4}$$

where

$$\gamma(r_L, L_u) = -\frac{\exp(-L_u/\lambda) - r_L \Gamma_b/\Gamma_a}{\exp(L_u/\lambda) - r_L \Gamma_b/\Gamma_a}. \tag{A.5}$$

Taking the $L \gg \lambda$ limit of (A.2) and substituting into the expression above for $\gamma(r_L, L_u)$ we obtain

$$\gamma(r_L, L_u) = \gamma(L_l, L_u) = -\frac{0.5\exp((-L_u + L_l)/\lambda) - 1}{0.5\exp((L_u + L_l)/\lambda) - 1}. \tag{A.6}$$

Rewriting in terms of L and p and taking the limit $pL \gg \lambda$ we get

$$\gamma(L) \approx 2\exp(-2L/\lambda). \tag{A.7}$$

Finally, using (A.3) and (A.4) and taking the limit $pL \gg \lambda$ once again we obtain

$$\delta\left(\frac{x_{r_L}}{L}\right) \approx \frac{1 + \frac{\lambda}{pL}\frac{\ln 2}{2}}{1 + 1/p} \tag{A.8}$$

$$\approx \frac{p}{1+p}, \tag{A.9}$$

which is the large-L limit of the curves in figure 4(*b*).

Glossary

Pattern scaling. Typically genes are expressed in well-defined regions of a developing field. The boundaries of these regions, determined by morphogen gradients, need to be placed at the correct position in the developing field; incorrect placement can result in death. The correct position is a certain fraction of the developing field size, which may vary by up to 20%. Pattern scaling refers to the ability of the embryo to adjust its boundaries of expression x such that when normalized by the size of the corresponding developing field L the ratio x/L has a spread about the functional value of, say, no more than 5%, i.e. $\delta(x/L) \leqslant 0.05$.

Bicoid. *Bicoid* mRNA is deposited by the mother in the *Drosophila* embryo and localized to the anterior region where it is translated soon after the egg is laid. The Bicoid protein can diffuse along the anterior–posterior axis, giving rise to a concentration gradient with its highest point at the anterior pole. Bcd is a homeodomain transcription factor that activates zygotic transcription in the embryo. The Bicoid gradient is the prototypical morphogen gradient [7].

Combinatorial model. A generic model in which the concentrations of a combination of morphogens (the input) determine the expression level of one or more target genes (the output). That part of the DNA where the morphogens bind is called a cis-regulatory module; a target gene may have multiple independent modules. The morphogens positively or negatively regulate the recruitment of the basal transcription machinery to the core promoter.

Annihilation model. In the annihilation model only one of the morphogens, say A, regulates the expression level of the target gene. The second morphogen B binds to A forming a product A_* which is unable to activate transcription. If the reaction is irreversible then the steady-state dynamics of A_* decouples from that of A and B which in turn becomes describable by the simpler annihilation reaction $A + B \to \emptyset$.

References

[1] Eldar A, Shilo B-Z and Barkai N 2004 Elucidating mechanisms underlying robustness of morphogen gradients *Curr. Opin. Gen. Dev.* **14** 435

[2] Houchmandzadeh B, Wieschaus E and Leibler S 2002 Establishment of developmental precision and proportions in the early *Drosophila* embryo *Nature* **415** 798

[3] Wolpert L 1969 Positional information and the spatial pattern of cellular differentiation *J. Theor. Biol.* **25** 1

[4] Driever W and Nüsslein-Volhard C 1988 The *bicoid* protein determines position in the *Drosophila* embryo in a concentration-dependent manner *Cell* **54** 95

[5] Gerland U, Moroz J D and Hwa T 2002 Physical constraints and functional characteristics of transcription factor-DNA interaction *Proc. Natl Acad. Sci. USA* **99** 12015

[6] Aegerter-Wilmsen T, Aegerter C M and Bisseling T 2005 Model for the robust establishment of precise proportions in the early *Drosophila* embryo *J. Theor. Biol.* **234** 13

[7] Ephrussi A and St Johnston D 2004 Seeing is believing: the Bicoid morphogen gradient matures *Cell* **116** 143

[8] Eldar A, Dorfman R, Weiss D, Ashe H, Shilo B-Z and Barkai N 2002 Robustness of the BMP morphogen gradient in *Drosophila* embryonic patterning *Nature* **419** 304

[9] Gregor T, Bialek W, de Ruyter van Steveninck R R, Tank D W and Wieschaus E F 2005 Diffusion and scaling during early embryonic pattern formation *Proc. Natl Acad. Sci. USA* **102** 18403

[10] Bollenbach T, Kruse K, Pantazis P, González-Gaitán M and Jülicher F 2005 Robust formation of morphogen gradients *Phys. Rev. Lett.* **94** 018103

[11] Yucel G and Small S 2006 Morphogens: precise outputs from a variable gradient *Curr. Biol.* **16** R29

[12] Jaeger J *et al* 2004 Dynamic control of positional information in the early *Drosophila* embryo *Nature* **430** 368

[13] Ochoa-Espinosa A, Yucel G, Kaplan L, Pare A, Pura N, Oberstein A, Papatsenko D and Small S 2005 The role of binding site cluster strength in Bicoid-dependent patterning in *Drosophila Proc. Natl Acad. Sci. USA* **102** 4960

[14] Small S, Blair A and Levine M 1992 Regulation of even-skipped stripe-2 in the *Drosophila* embryo *EMBO J.* **11** 4047

[15] Bintu L, Buchler N E, Garcia H G, Gerland U, Hwa T, Kondev J and Phillips R 2005 Transcription regulation by the numbers: models *Curr. Opin. Gen. Dev.* **15** 116

[16] Howard M and ten Wolde P R 2005 Finding the center reliably: robust patterns of developmental gene expression *Phys. Rev. Lett.* **95** 208103
[17] Houchmandzadeh B, Wieschaus E and Leibler S 2005 Precise domain specification in the developing *Drosophila* embryo *Phys. Rev.* E **72** 061920
[18] Lucchetta E M, Lee J H, Fu L A, Patel N H and Ismagilov R F 2005 Dynamics of *Drosophila* embryonic patterning network perturbed in space and time using microfluidics *Nature* **434** 1134
[19] Buchler N E, Gerland U and Hwa T 2003 On schemes of combinatorial transcription logic *Proc. Natl Acad. Sci.* **100** 5136
[20] Eldar A, Rosin D, Shilo B-Z and Barkai N 2003 Self-enhanced ligand degradation underlies robustness of morphogen gradients *Developmental Cell* **5** 635
[21] Ben-Naim E and Redner S 1992 Inhomogeneous two-species annihilation in the steady state *J. Phys. A: Math. Gen.* **25** L575
[22] Schroeder M D, Pearce M, Fak J, Fan HQ, Unnerstall U, Emberly E, Rajewsky N, Siggia E D and Gaul U 2004 Transcriptional control in the segmentation gene network of *Drosophila PLoS Biol.* **2** e271
[23] Ma X, Yuan D, Diepold K, Scarborough T and Ma J 1996 The *Drosophila* morphogenetic protein Bicoid binds DNA cooperatively *Development* **122** 1195
[24] Zamore P D, Bartel D P, Lehmann R and Williamson J R 1999 The Pumilio–RNA interaction: a single RNA-binding domain monomer recognizes a bipartite target sequence *Biochemistry* **38** 596
[25] Crauk O and Dostatni N 2005 Bicoid determines sharp and precise target gene expression in the *Drosophila* embryo *Curr. Biol.* **15** 1888
[26] St Johnston D, Beuchle D and Nüsslein-Volhard C 1991 *Staufen*, a gene required to localize maternal RNAs in the *Drosophila* egg *Cell* **66** 51
[27] Ferrandon D, Elphick L, Nüsslein-Volhard C and St Johnston D 1994 Staufen protein associates with the 3'UTR of *bicoid* mRNA to form particles that move in a microtubule-dependent manner *Cell* **79** 1221
[28] Fu D and Ma J 2005 Interplay between positive and negative activities that influence the role of Bicoid in transcription *Nucl. Acids Res.* **33** 3985